Dynamics of shear-induced orientation transitions in block copolymers

J. Stasiak,*[a] M. R. Mackley,[a] A. M. Squires,[b] V. Castelletto,[b] I. W. Hamley[b] and G. D. Moggridge[a]

Received 15th January 2010, Accepted 2nd March 2010
First published as an Advance Article on the web 22nd March 2010
DOI: 10.1039/c000975j

This research investigates the dynamics of mechanical and structural transformations of styrene–butadiene–styrene block copolymer, known as RCM1, which has cylindrical mesophase morphology. The polymer was processed using a Multipass Rheometer (MPR) with simultaneous X-ray observation. The method allowed investigation of the dynamics with 1 second time resolution. Samples were processed at 160 °C and an apparent wall shear rate in the range ~1.4 to 1125 s^{-1}. Microstructural alignment was quantified using a second order X-ray orientation function. The polymer showed self-organization in the melt, aligning along the capillary walls. Shear flow disrupted the organization, which then rebuilt during the post-shearing pause, as the residual pressure relaxed across the capillary. The dynamics of structure ordering and disordering was a function of shear rate. The transition was faster for high shear rate cycles.

Introduction

Emerging research suggests polymeric systems as templates for uniform nanostructures and field-responsive materials with switchable molecular orientation. Particularly useful materials are block copolymers, which behave as thermoplastic elastomers or glassy modified rubber materials, at temperatures between the glass transition temperatures of the blocks. The performance of these materials is critically dependent on their flow properties and resultant morphologies. Thus it is beneficial to gain understanding of the microstructures that persist after processing, as well as of their evolution during and after flow. The flow induced behaviour of polymer may be studied in terms of molecular alignment, which typically involves the orientation of nanoscale domains. Depending on shear rate, processing may induce or reduce microstructure ordering in block copolymers.[1] To monitor the structural development during processing a method combining rheology and direct structural characterisation needs to be applied. A variety of rheo-optic probes have been extensively studied, such as birefringence,[2–7] light scattering,[8–10] X-ray scattering[11–20] and SANS.[21–23] However, to study the dynamics of the deformation process a fast probing method like, for example, the high flux of a synchrotron source should be applied. Such studies usually require special design of a flow cell with good control over thermal conditions and mechanical performance. An example is the plate–plate rheometer design by Keates *et al.*[12] for *in situ* synchrotron study of global orientation in liquid crystalline systems.

In this work we perform simultaneous capillary flow-SAXS experiments on a styrene–butadiene–styrene (SBS) block copolymer forming butadiene cylinders. We present a method that achieves an increase of time resolution of X-ray probing during cyclical deformation. Results are concerned with the domain orientation within the copolymer during and after flow and also the influence of shear rate on the dynamics of structural change.

Experimental

We used an SBS block copolymers from BASF called RCM1. The copolymer morphology below T_{ODT}, which is over 200 °C, is polybutadiene rich cylinders in a polystyrene matrix. The volume fraction of polystyrene is 74%. The molecular weight is around 100 000 g mol^{-1} and polydispersity about 1.2. Polymer was provided in pellet form and processed at 160 °C in a multi-pass rheometer (MPR) without prior purification.

A detailed description of the Cambridge MPR can be found in the work of Mackley *et al.*[24] The MPR, a schematic of which is shown in Fig. 1, consists of two pistons, located in the top and bottom barrels. The reciprocating pistons enclose a fixed volume of the sample and push it backwards and forwards through a central test section, such as a capillary. High precision servo-hydraulics control the displacement of the pistons and their positions are monitored by linear displacement transducers. Pressure transducers, on either side of the capillary, enable

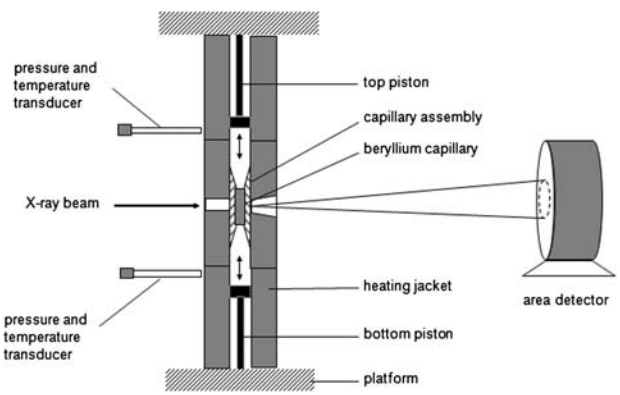

Fig. 1 Schematic of Cambridge Multipass Rheometer with an *in situ* XRD measurement facility (MPR3).

[a]*Department of Chemical Engineering and Biotechnology, University of Cambridge, Cambridge, CB2 3RA, UK. E-mail: js744@cam.ac.uk*
[b]*Department of Chemistry, University of Reading, Reading, RG6 6AD, UK*

time-dependent differential pressure measurements to be made from which rheological parameters can be determined. The sample temperature is controlled by circulating heating oil in the jackets around the barrels and the test section.

For X-ray examination, the central section of the MPR was an X-ray transparent beryllium capillary as shown in Fig. 1. The MPR barrel section is able to fit in our X-ray unit allowing simultaneous rheology and X-ray measurements.[25–27] SAXS patterns were recorded using a Bruker analytical X-ray system. CuKα lab source with $\lambda = 1.54$ Å was generated by a Siemens ceramic tube operated at 45 kV and 45 mA. The beam was collimated by a three pinhole collimator, and the specimen was placed 70 mm from the HiStar 2-D multiwire detector. Bruker SAXS data collection and analysis software were used.

The apparent wall shear rate was calculated by the standard relations for Poiseuille flow:

$$\gamma_w = \frac{4Q}{\pi r^3} \quad (1)$$

where Q is volumetric flow rate and r is capillary radius. The uncorrected wall shear stress was calculated from the measured drop in steady state pressure:

$$\tau_w = \frac{r\Delta P}{2L} \quad (2)$$

where L is length of the capillary. Depending on piston velocity and capillary geometry we were able to follow material structural changes over a wide range of apparent wall shear rates. Our experiments were performed for piston speeds between 0.05–5 mm s^{-1} and we used 2 mm and 4 mm diameter capillaries covering shear rates from 1.4 s^{-1} to 1125 s^{-1}.

To complement the results an assembly with a slit geometry in the MPR with an optical configuration was used. This technique has been previously described by several authors.[28–30] During experiments, the pistons were moved in synchrony, forcing the material to flow in the midsection within the contraction geometry of the slit, schematically presented in Fig. 2. Monochromatic polarized light with a wavelength of 514 nm was passed through the midsection and orthogonal analyzer, and images were captured using a digital video camera. Quarter-wave plates were used to eliminate the isoclinic extinction bands to leave only the stress and orientation related isochromatic fringes. The optical train consisted of: polariser lens at 0°, quarter-wave plate at 45°, sample between quartz windows, quarter-wave plate at 135° and analyser lens at 90°.

To investigate the dynamics of microstructure changes during processing we applied a time resolved technique described by Cooney *et al.*[31] The method is based on collection of many short X-ray exposures over many repetitions of the same deformation cycle. The overall X-ray image was a sum of frames taken in the same cycle step.

In multipass mode, the pistons reciprocate in tandem at a set speed and for a set displacement with rest time between each stroke. Each of the two flow periods in a cycle is associated with a different flow direction, see Fig. 3. During MPR processing a series of short exposures were taken over many cycles, started with the pistons moving down after a pause section. We were able to collect as short as 1s X-ray exposures containing very few counts each. The time when each frame was taken was compared after the experiment with a record of the position of the pistons with time. After processing, frames taken at the same piston positions over the cycle were added together into one bin giving one overall image, containing many counts and suitable for further analysis. The number of repetitions of the cyclic process was chosen to standardise the total collection time of all frames in the bin to 600 s. The method allows the study of the dynamics of structure transformation with time resolution much better than conventional lab X-ray scattering methods.

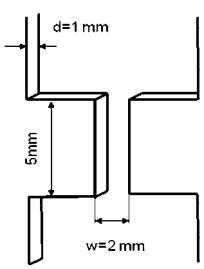

Fig. 2 Schematic of slit geometry for optical experiments.

Results and discussion

X-Ray experiments

Although X-ray scattering probes the structure at the molecular level, the resultant patterns represent an average over the molecules in a volume defined by the incident beam. The orientation is characterized by the average direction of domains and average direction of the lattice planes. In order to obtain orientation parameters from X-ray scattering pattern we must consider the azimuthal variation of intensity at a fixed polar angle θ. In this context the degree of orientation can be quantified by the second order orientation function:

$$P_2 = C^{-1}(3 \times \langle \cos^2 \chi \rangle - 1)/2 \quad (3)$$

where χ is the azimuthal angle and $\langle \cos^2 \chi \rangle$ denotes the average of $\cos^2 \chi$, which is given by

$$\langle \cos^2 \chi \rangle = \frac{\int_0^{\pi} I(\theta,\chi) \cos^2(\chi) \sin(\chi) \mathrm{d}\chi}{\int_0^{\pi} I(\theta,\chi) \sin(\chi) \mathrm{d}\chi} \quad (4)$$

$I(\theta,\chi)$ represents the scattered intensity at polar angle θ and azimuthal angle χ. We define χ to be zero along a line parallel to

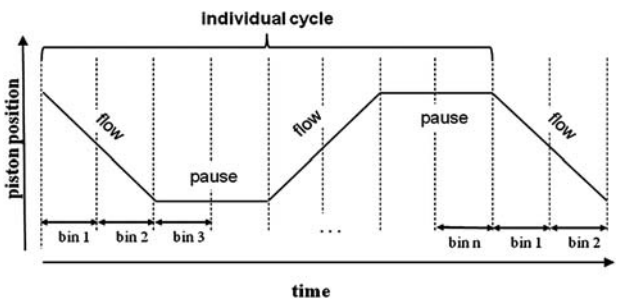

Fig. 3 Diagram of time stamped cycle. Length of a bin represents time of an individual X-ray frame.

the flow direction. Orientation of cylinders parallel to the flow results in preferential scattering at $\chi = \pi/2$ and $3\pi/2$ rather than $\chi = 0$ or π (Fig. 4a). Therefore we apply the conversion constant C[32,33]

$$C = (3\cos^2 \Phi - 1)/2 \quad (5)$$

in which Φ denotes the angle of the cylinders to the normal to the flow direction and becomes 90° (or 270°), hence $C = -1/2$.

An orientation function P_2 so defined has a value of 1 for a perfectly uniaxially oriented structure, while a completely isotropic sample is characterized by $P_2 = 0$.

Fig. 4a shows SAXS patterns collected from continuous exposures for 600 s. To eliminate the influence of forward beam scattering, a background pattern was collected separately and subtracted from the data. We observed that before processing in the MPR, RCM1 in the molten state at 160 °C is oriented; two equatorial reflections indicate orientation along the capillary length. The orientation was eliminated when the polymer was subjected to high shear. The pattern contains low counts and shows uniform scattering indicating no preferential orientation. Continuous X-ray scattering of the shearing experiment was performed for shear rate 1125 s^{-1}. For this experiment pistons moved in conjunction up and down without any pause. After cessation of the shear the diffraction pattern again develops anisotropy within the sample. The experiment demonstrates that the preferential microstructure of static RCM1 at the applied temperature and geometry is oriented parallel to the capillary walls.

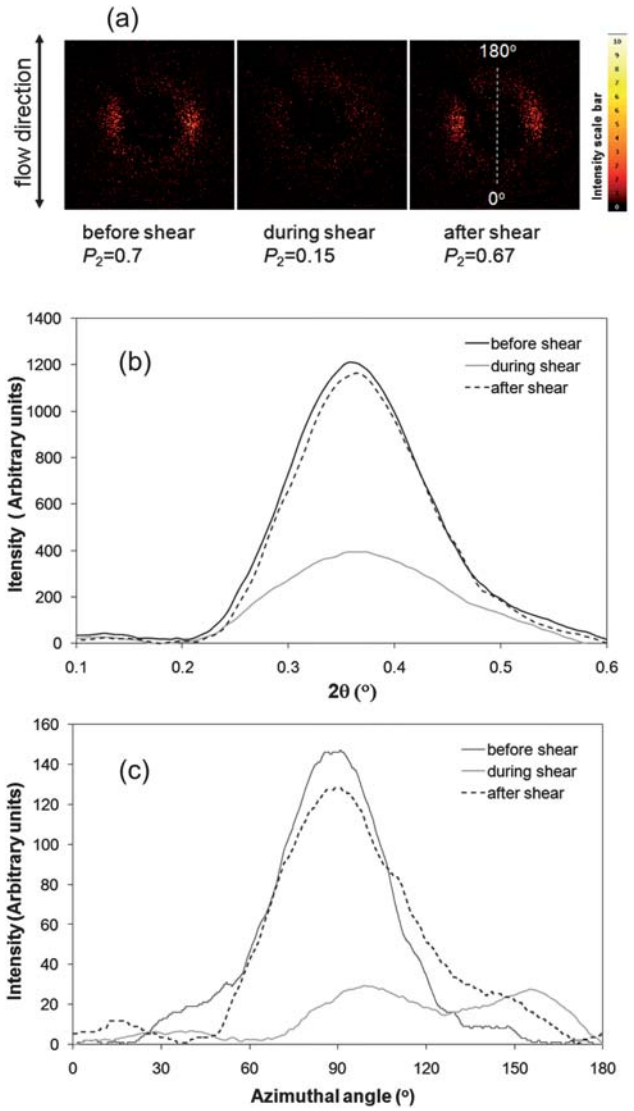

Fig. 4 (a) SAXS profile of RCM1 before shear, during continuous shear at rate 1125 s^{-1} and 10 min after shear cessation, (b) scattered intensity as a function of polar angle over the range of $\chi = 0$–360° and $2\theta = 0.1$–0.6°, (c) scattered intensity as a function of azimuthal angle over the range of $\chi = 0$–180° and $2\theta = 0.25$–0.5°.

Scattered intensity profiles as a function of polar and azimuthal angle are shown in Fig. 4b and c respectively. The SAXS pattern has the primary scattering peak at $2\theta = 0.36°$ corresponding to a d spacing of 24.5 nm from hexagonally ordered polybutadiene rich cylinders. The azimuthal anisotropy quantified by P_2 for the molten sample before shear was 0.7, while the sample sheared continuously had $P_2 = 0.15$. Sample scattered 10 minutes after shear had an orientation function of 0.67, confirming a return to initial alignment.

To probe the dynamics of transformation of the structure between lower and higher ordered states, a series of time resolved experiments have been completed. The polymer was processed in cycles consisting of two flow and two pause periods as shown in Fig. 3. Processing conditions are described by piston velocity in mm s^{-1}, amplitude in mm and dwell period in s. Following the characterization, cycles were denoted by 3 numbers (for example '5–10–18'). The first number represents pistons velocity (5 mm s^{-1}), the second—the amplitude (10 mm) and the third—the pause (18 s).

Fig. 5 presents the time resolved orientation function for RCM1 processed in high, medium and low shear rate regimes. The data are complemented by experimentally and numerically obtained pressure traces across the capillary. The capillary flow model incorporating melt compressibility is based on the work of Ranganathan *et al.*,[34]

$$\frac{d\Delta P}{dt} = \frac{1}{\chi}\left(\frac{1}{V_t} + \frac{1}{V_b}\right)\left(\pi R^2 u_p - a(\Delta P)^b\right) \quad (6)$$

where χ is the melt compressibility, V_t and V_b are volumes of top and bottom barrels, R is radius of the barrels, u_p is piston velocity, a and b are constants of power-low flow equation $Q = a(\Delta P)^b$, which were derived from experimental flow curves. According to the model when the pistons start moving the difference in pressure increases and reaches a steady state value. When the pistons stop, the pressure difference decreases rapidly but before it can relax completely the next cycle begins after the rest time. Relaxation of the pressure difference across the capillary can be attributed to flow in the capillary associated with pressure equalization in both barrels.

The measured traces at the beginning of flow differed slightly from the modelled, demonstrating delayed increase of the pressure. The MPR consists of sections of different diameters: barrels of diameter 15 mm and capillaries of diameter either 2 mm or 4 mm. Thus the flow of the viscous fluid in the region of the diameter change was accompanied by volume contraction. After reaching the critical volume at the entrance of the capillary the polymer started to flow.

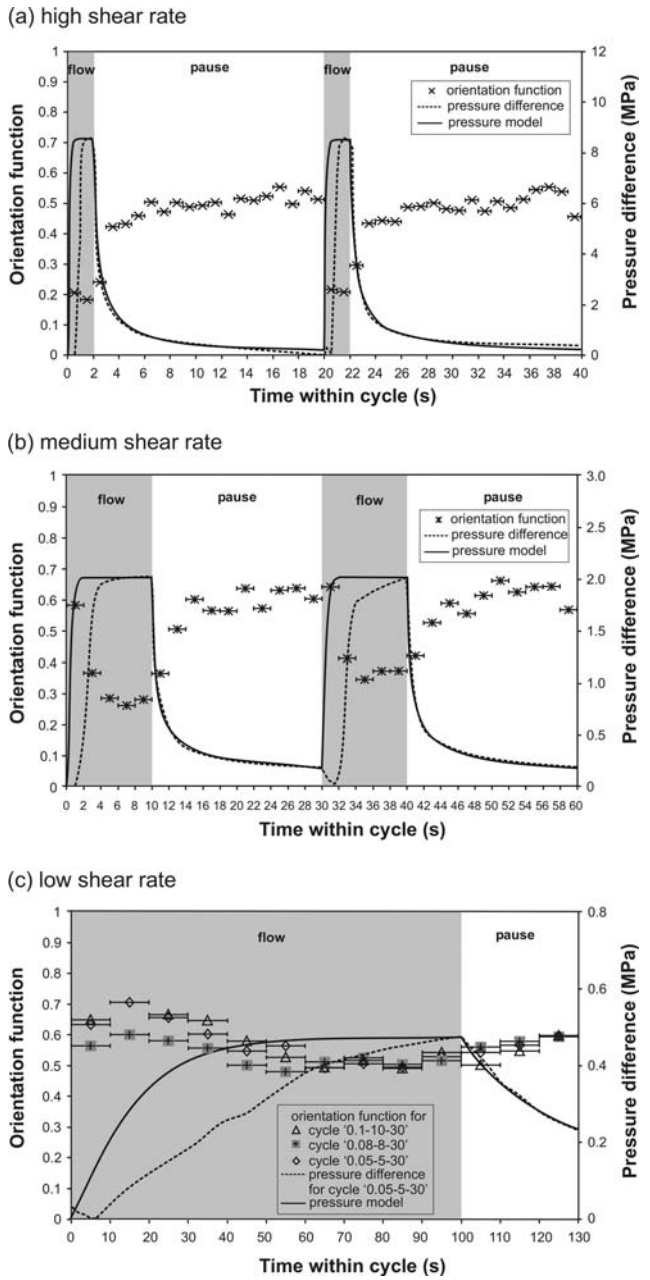

Fig. 5 Orientation function and differential pressure for RCM1 processed in (a) high shear rate regime: cycle '5–5–18', apparent wall shear rate 1125 s^{-1}, (b) medium shear rate regime: cycle '1–10–20',apparent wall shear rate 28 s^{-1}, (c) low shear rate regime: apparent wall shear rate 2.8 s^{-1} for cycle 0.1–10–30, 2.25 s^{-1} for cycle 0.08–8–30 and 1.4 s^{-1} for cycle 0.05–5–30. Experimental pressure difference is compared with predictions of compressible flow model by Ranganathan *et al.*[34]

Further piston displacement was directly related to flow. However, the observed delay of pressure response, which is typical for a highly compressible medium, may suggest in addition to polymer compressibility, the presence of air trapped between polymer pellets during loading of the material into the MPR.

Calculated time resolved orientation data exhibited an inverse relation to measured differential pressure in the MPR. P_2 dropped when differential pressure increased and the orientation was rebuilt again during pressure relaxation. The values of orientation function for RCM1 processed in cycle '5–5–18' (Fig. 5a), at high wall shear rate (1125 s^{-1}) are in agreement with the previous work,[31] where individual frames were collected for 5 s. Our data represent higher time resolution, 1 s frames. The data reveal a trend of decreasing P_2 values during flow and increasing orientation in the pause period. The transformation to higher orientation after cessation of flow is accomplished in about 1 s, which can be determined due to the enhanced time resolution achieved in this work. However, the maximum orientation function values were about 0.55, indicating that longer recovery time is necessary to restore the initial preferential orientation ($P_2 \approx 0.7$). Given the evidence in the literature for shear orientation, it is believed that the low shear rates generated by pressure relaxation are responsible for the phase alignment after processing ceases.

Results for cycles processed at medium shear rates are presented in Fig. 5b. Similarly to the previous data we observed lower orientation during flow and higher P_2 values in the pause period. However, some changes in orientation during flow are also evident. Due to polymer compressibility, the first stage of flow performed at low shear rate did not destroy the orientation reached during the pause period. Orientation dropped noticeably only after 4 s of piston movement, when the pressure significantly increased. The time to establish higher orientation after flow cessation was longer in this case, about 4–6 s.

The low shear rate experiments required low piston velocity, which extended the overall cycle time. Thorough probing of a long cycle with high time resolution involves many hours of data collection and produces thousands of files for processing. Assuming symmetry in a whole cycle, frames taken in the first-half of the cycle were combined with frames taken in the second-half of the cycle. Moreover in this case we expected to see slow structural changes; therefore the collection time for individual frames was extended to 10 s. This allowed significant shortening of the experiments, but the results could be presented for one flow and one pause period only (since "up" and "down" piston strokes have been treated as equivalent and combined).

The influence of low shear rate processing on microstructure of RCM1 is shown in Fig. 5c. The figure contains data collected in three cycles '0.1–10–30', '0.08–8–30' and '0.05–5–30' at apparent wall shear rate 2.8 s^{-1}, 2.25 s^{-1} and 1.4 s^{-1} respectively. Due to low velocities and the long timescale for the experiments, evidence of increase of orientation at the beginning of the flow period was captured, confirming a delay in the full development of flow. During this time the microstructure oriented further, beyond that achieved in the pause period. The maximum orientation was reached within 10–20 s of the start of the flow period. Then the P_2 function decreased, achieving minimum values at about 60–70 s of flow and remained stable to the end of the flow period. The orientation increased slightly again after the shear ceased. Moreover we noticed that the values of orientation function are inversely proportional to applied shear rate. However, in this case the P_2 function for flow and pause periods did not differ as much as for higher flow rate cycles.

To summarise the effect of shear on orientation, the time resolved orientation function has been presented in Fig. 6 as a function of wall shear stress, calculated from the measured difference in pressure according to eqn (2), at different piston

speeds. Most of the shear-induced order–disorder transition was observed for wall shear stress up to 150 000 Pa. Further increasing of the wall shear stress caused only slight variations of the orientation function.

While the shear induced ordering mechanism has been widely discussed in literature,[15,35,36] shear-induced disorder has not been explained. A schematic diagram shown in Fig. 7 clarifies both the microstructure and ordering within the MPR capillary during and after flow. There is evidence from these results that at high shear stress the polymer undergoes a microstructural instability leading to loss of orientation. Initially oriented cylinders lost order during compression at the entrance to the capillary. The compression, perpendicular to piston displacement direction, might initiate local perpendicular orientation and worm like molecular structure. After entering the capillary the polymer was subjected to a non-uniform velocity field, which caused further disruption of polymer organisation. As a consequence of these mechanisms affecting the polymer during the flow, the microstructure transformed to global disorder. As soon as the high shear stress relaxed, orientation was re-gained due to low shear flow governed by decompression. The orientation remained in the polymer even after complete relaxation indicating that the ordered state is stable for the polymer under the conditions investigated.

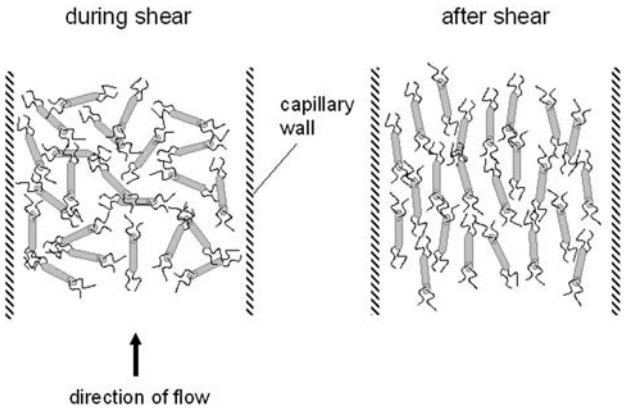

Fig. 7 Schematic of cylindrical mesophase structure formed by RCM1 in the MPR capillary during and after flow.

Birefringence

Flow induced birefringence is a well-established technique that allows visualisation of the principal stress difference generated by flow and hence identification of the stress distribution in the polymer. Birefringence is also one of the most sensitive probes of molecular orientation in polymers.[5,7] For instance, for polystyrene the measured birefringence increases linearly with molecular orientation.[37] To complement our X-ray based results we performed a series of optical observations of RCM1 processed in the MPR equipped with an optical cell. Temperature and shear rate conditions were equivalent to our X-ray experiments. The flow cell was bounded by quartz windows, containing a 2 mm wide and 1 mm deep slit as shown schematically in Fig. 2.

Birefringence, which can be seen during the shear flow, is an integral effect of both stress and orientation. Due to the coexistence of these two birefringence inducers, image interpretation, in terms of orientation only, is difficult: particularly at high shear rates the contribution of stress birefringence is very significant.

A sequence of images taken during a high shear rate cycle is shown in Fig. 8a. The shear rate of 1180 s^{-1} is equivalent to our '5–5–18' cycle in the X-ray experiments, see Fig. 5a. We observed intense bright birefringence during flow, which relaxed almost immediately after flow cessation and rapidly increased again, indicating the development of structural anisotropy during the pause period.

Fig. 8b presents selected frames for polymer processed at medium shear rate (118 s^{-1}), similar to the '4–12–12' cycle in the X-ray experiment. The flow induced birefringence relaxed almost completely in 20 s after the flow ceased. Then the structure

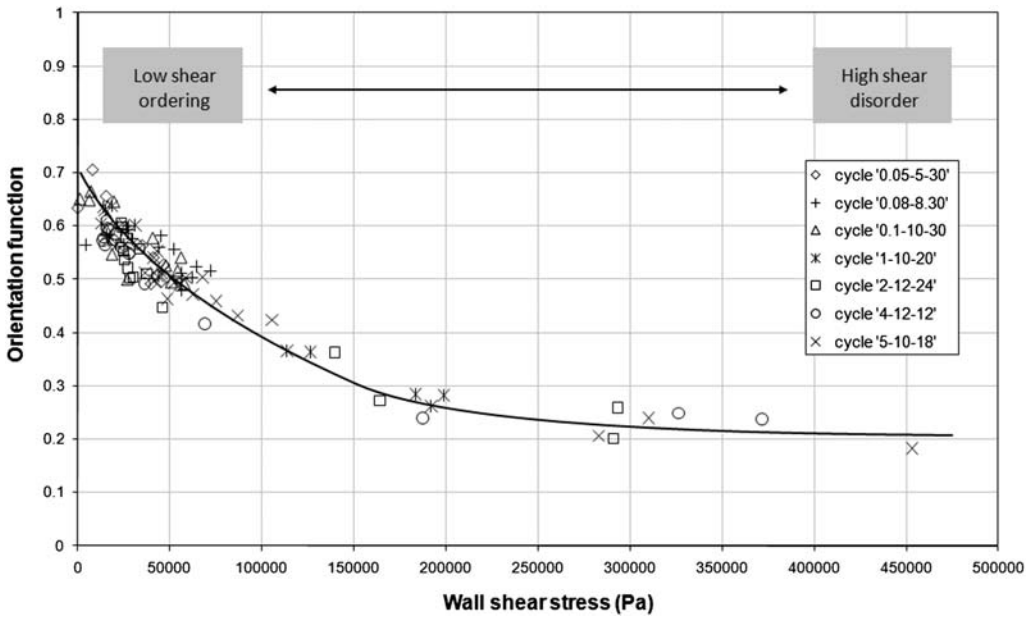

Fig. 6 Orientation function of RCM1 as a function of wall shear stress at 160 °C.

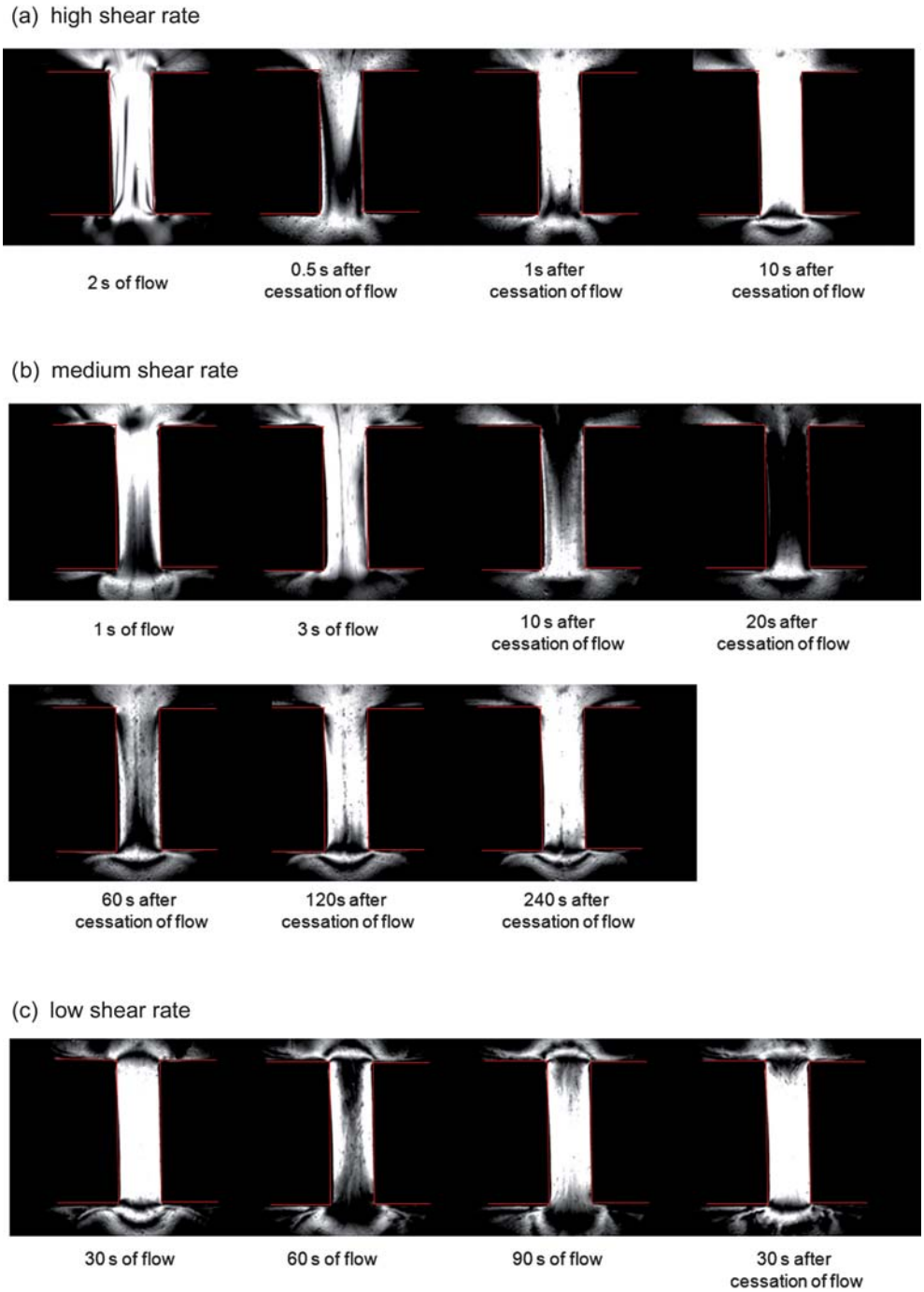

Fig. 8 Observation of RCM1 processed at (a) high shear rate; 1180 s^{-1}, (b) medium shear rate; 118 s^{-1} and (c) low shear rate; 2.3 s^{-1}.

started to build up orientation starting from the slit walls and expanding to the whole cell volume in about 4 minutes. This is particularly interesting due to easily distinguishable stress and orientation caused birefringence. Additionally the timescale of the structural changes is long enough for detailed observations. The long-time structural transformation is consistent with a slow return to the "steady–state" quiescent orientation function of 0.7 determined by X-ray scattering.

Birefringence images shown in Fig. 8c represent the low shear rate case (2.3 s^{-1}), similar to that achieved in cycle '0.08–8–30'. Due to low velocity, flow birefringence could not be identified. We can assume that the strong birefringence is a result of high structural anisotropy. Flow slightly reduces the anisotropy but it is quite rapidly rebuilt after flow cessation.

Whilst quantification of birefringence would be desirable, it is particularly difficult for this material. The observed birefringence originates from two sources. The material can show an intrinsic birefringence associated with its local orientation and additional birefringence associated with flow. In both cases it is not possible to obtain a perfectly ordered birefringence value and consequently it is not possible to extract an overall or local P_2 for the intrinsic or flow induced birefringence.

Conclusions

This study presents the effect of shear rate on microstructure of RCM1, as well as on post-shearing domain order. Increased temporal resolution of X-ray measurements during cyclic processing, achieved by a frame binning method, allowed the observation of the dynamics of structural transformations.

The results observed in this study differ from the majority of reports describing orientation induced by shear flow in polymeric systems.[3,4,14,38–40] The fundamental difference is that the initial state of microstructure, prior to shear flow was highly oriented. Thus, the origin of the decrease of P_2 with shear rate is here very different from the case of purely isotropic solutions and is a complex mechanism resulting from initial morphology and shear history of the melt.

The analysis of time resolved X-ray patterns in terms of the orientation parameter shows that orientation is a function of wall shear stress. All values are in range 0.15–0.7, bracketed by P_2 for sample sheared continuously and P_2 for a sample before processing. The shear flow introduces disordering that is progressive with the amount of applied shear stress. The textural changes are reversible and the orientation returns when the shear stress is decreased. Most of the order–disorder transition is complete within the range of wall shear stress up to 150 000 Pa. Dynamics of the transition depends on shear rate and was faster for high shear rate cycles.

The rheo-optic experiments gave an insight into stress and orientation birefringence and complemented the X-ray tests. Ordered RCM1 does not spontaneously lose alignment when the shear field is removed. Anisotropic X-ray patterns as well as birefringence observations after the application of shear are thus reliable indicators of ordered phase stability in static polymer. The optical experiments also demonstrated the development of order during the pause period from the capillary wall and propagating into the polymer bulk. This is consistent with the timescale of ordering after the cessation of flow observed in the X-ray experiments.

The complementary experiments presented here give a consistent picture of the phase structure of RCM1 during and post-flow.

Acknowledgements

The authors thank the EPSRC for financial support for this work under Grants EP/F007663/1 and EP/F007795/1.

References

1 N. P. Balsara and H. J. Dai, *J. Chem. Phys.*, 1996, **105**, 2942.
2 K. Amundson, E. Helfand, S. S. Patel and X. Quan, *Macromolecules*, 1992, **25**, 1935.
3 V. K. Gupta, R. Krishnamoorti and J. A. Kornfield, *Macromolecules*, 1995, **28**, 4464.
4 V. K. Gupta, R. Krishnamoorti, J. A. Kornfield and S. D. Smith, *Macromolecules*, 1996, **29**, 1359.
5 H. Wang, M. C. Newstein, M. Y. Chang, N. P. Balsara and B. A. Garetz, *Macromolecules*, 2000, **33**, 3719.
6 F. M. Abuzaina, B. A. Garetz, J. U. Mody, M. C. Newstain and N. P. Balsara, *Macromolecules*, 2004, **37**, 4185.
7 F. M. Abuzaina, A. J. Patel, S. Mochrie, S. Narayanan, A. Sandy, B. A. Garetz and N. P. Balsara, *Macromolecules*, 2005, **38**, 7090.
8 H. Siebert, I. Quijada-Garrido, J. Vermant, L. Noirez, W. R. Burghardt and C. Schmidt, *Macromol. Chem. Phys.*, 2007, **208**, 2161.
9 T. Kume, T. Hashimoto, T. Takahashi and G. G. Fuller, *Macromolecules*, 1997, **30**, 7232.
10 E. C. Lee, M. J. Solomon and S. J. Muller, *Macromolecules*, 1997, **30**, 7313.
11 H. H. Winter, D. B. Scott, W. Gronski, S. Okamoto and T. Hashimoto, *Macromolecules*, 1993, **26**, 7236.
12 P. Keates and G. R. Mitchell, *J. Non-Newtonian Fluid Mech.*, 1994, **52**, 197.
13 S. Okamoto, K. Saijo and T. Hashimoto, *Macromolecules*, 1994, **27**, 5547.
14 J. A. Pople, I. W. Hamley, J. Patrick, A. Fairclough, A. J. Ryan and C. Booth, *Macromolecules*, 1998, **31**, 2952.
15 W. J. Zhou, J. A. Kornfield, V. M. Ugaz, W. R. Burghardt, D. R. Link and N. A. Clark, *Macromolecules*, 1999, **32**, 5581.
16 S. Stangler and V. Abetz, *Rheol. Acta*, 2003, **42**, 569.
17 V. Castelletto, P. Parras, I. W. Hamley, P. Davidson, J. Yang, P. Keller and M. H. Li, *Macromolecules*, 2005, **38**, 10736.
18 S. Rendon, W. R. Burghardt, M. L. Auad and J. A. Kornfield, *Macromolecules*, 2007, **40**, 6624.
19 E. Verploegen, L. C. McAfee, L. Tian, D. Verploegen and P. T. Hammond, *Macromolecules*, 2007, **40**, 777.
20 V. Castelletto, A. M. Squires, I. W. Hamley, J. Stasiak and G. D. Moggridge, *Liq. Cryst.*, 2009, **36**, 435.
21 F. A. Morrison, M. Muthukumar, A. I. Nakatani and C. C. Han, *Macromolecules*, 1993, **26**, 5271.
22 R. Muller, J. J. Pesce and C. Picot, *Macromolecules*, 1993, **26**, 4356.
23 H. Wang, M. C. Newstein, A. Krishnan, N. P. Balsara, B. A. Garetz, B. Hammouda and R. Krishnamoorti, *Macromolecules*, 1999, **32**, 3695.
24 M. R. Mackley, R. T. J. Marshall and J. B. A. F. Smeulders, *J. Rheol.*, 1995, **39**, 1293.
25 M. R. Mackley, G. D. Moggridge and O. Saquet, *J. Mater. Sci.*, 2000, **35**, 5247.
26 A. Lele, M. Mackley, G. Galgali and C. Ramesh, *J. Rheol.*, 2002, **46**, 1091.
27 S. A. McKeown, M. R. Mackley and G. D. Moggridge, *Trans. IChemE*, 2003, **81**, 649.
28 M. W. Collis and M. R. Mackley, *J. Non-Newtonian Fluid Mech.*, 2005, **128**, 29.
29 K. D. Coventry and M. R. Mackley, *J. Rheol.*, 2008, **52**, 401.
30 L. Scelsi and M. R. Mackley, *Rheol. Acta*, 2008, **47**, 895.
31 D. T. Cooney, J. P. DeRocher, G. D. Moggridge and A. M. Squires, *J. Mater. Sci.*, 2007, **42**, 9663.
32 J. Y. Lee, M. S. Park, H. C. Yang, K. Cho and J. K. Kim, *Polymer*, 2003, **44**, 1705.
33 S. Sakuari, S. Aida, S. Okamoto, T. Ono, K. Imaizumi and S. Nomura, *Macromolecules*, 2001, **34**, 3672.
34 M. Ranganathan, M. R. Mackley and P. H. J. Spitteler, *J. Rheol.*, 1999, **43**, 443.
35 D. B. Scott, A. J. Waddon, Y. G. Lin, F. E. Karasz and H. H. Winter, *Macromolecules*, 1992, **25**, 4175.
36 M. E. Vigild, C. Chu, M. Sugiyama, K. A. Chaffin and F. S. Bates, *Macromolecules*, 2001, **34**, 951.
37 A. D. Gabaraeva, M. F. Milagin and N. I. Shishkin, *Mekh. Polim.*, 1967, **3**, 1105.
38 F. A. Morrison and H. H. Winter, *Macromolecules*, 1989, **22**, 3533.
39 S. Kitade, N. Ochiai, Y. Takahashi, I. Noda, Y. Matsushita, A. Karim, A. I. Nakatani, H. Kim and C. C. Han, *Macromolecules*, 1998, **31**, 8083.
40 W. K. Lee, H. D. Kim and E. Y. Kim, *Curr. Appl. Phys.*, 2006, **6**, 718.